**THE EUROPEAN
PHYSICAL JOURNAL D**

Regular Article – Plasma Physics

Light emission processes in the context of optical beam profile monitors

Raphael Hampf[1,a], Jochen Wieser[2,b], and Andreas Ulrich[1,c]

[1] Physik-Department, Technische Universität München, James-Franck-Str. 1, 85748 Garching bei München, Germany
[2] Excitech GmbH, Branterei 33, 26419 Schortens, Germany

Abstract. Light emission from gas targets using heavy ion beam excitation is described. Typically ^{32}S beams with ≈ 90 MeV (2.8 MeV/amu) particle energy were used. This study was performed in context of optical beam profile measurements. Optical transitions from neutral and singly ionized rare gases are suggested for this application. Emission spectra and their line intensities are presented for a wide range of target pressures from about 10^{-5} to 300 mbar. The effect of secondary electrons on the beam profiles is discussed. A comparison of ion beam and electron beam-induced spectra is shown and interpreted by a semi-quantitative model of the excitation mechanisms. Examples of beam profiles recorded with three different cameras through appropriate optical filters are presented. A comparison of projected profiles and radial profiles obtained by Abel inversion is given. Effective emission cross sections were measured for atomic and ionic lines at various target gas pressures and their pressure dependence interpreted by the excitation mechanisms. Examples of time-resolved measurements of light emission following pulsed excitation support the interpretation of the excitation mechanisms discussed in this overview of ion beam-induced light emission of gas targets.

1 Introduction

Particle accelerators are an important tool for both basic research and applications. Projectiles from an electron or ion source are accelerated and transported to a target. The projectiles are guided from the source to the target by electrostatic or magnetic lenses and steerers, analogue to optical imaging. This has to be controlled by an appropriate beam diagnostics. Mechanical elements like grids, wires or scintillating plates are normally used for that purpose. However, modern accelerators often work with high-beam currents which can destroy the beam diagnostic elements. Optical beam diagnostics can avoid this problem. In that case a low-pressure gas is filled into a section of the beamline, the beam excites the gas atoms or molecules in inelastic collisions, and a following light emission is observed with cameras (Fig. 1). This allows observing beam position and transverse beam profiles [1–4].

This study is motivated by the new ion accelerator under construction at the GSI/ FAIR project in Darmstadt, Germany, with intensities demanding for optical diagnostics. The facility will work with high-beam currents both in the injector and in a large synchrotron, where optical methods are considered, e.g., for alignment and beam focus-profile determination in plasma physics experiments (HHT and APPA cave). In this work, a much smaller device, the Tandem van de Graaff accelerator at the Maier-Leibnitz-Laboratory Munich, was used for fundamental studies of ion beam-induced light emission. The goal was to further investigate gas species and spectral emission features well suited for optical beam diagnostics.

This work is based on experience with other applications of particle beam-induced light emission such as heavy ion beam-pumped gas lasers [5–11] and electron beam-pumped light sources [12–15]. It extends to much lower-target gas pressures compared to the earlier experiments.

Optical beam diagnostics appears to be very simple at first glance (Fig. 1). However, several effects lead to the fact that the light emission is not necessarily confined to the actual region where the primary beam is propagating. Here we discuss mainly secondary electrons emitted from the ion beam region leading to additional excitation and light emission around the primary beam. Other effects can be optical light trapping, diffusion of excited species, heating and expansion of the target gas, and for high energy collisions also effects of recoil ions [16].

[a] e-mail: raphael.hampf@tum.de

[b] e-mail: jochen.wieser@excitech.de

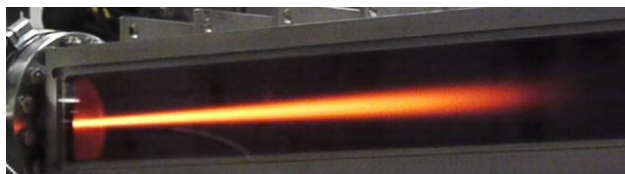[c] e-mail: andreas.ulrich@ph.tum.de (corresponding author)

Fig. 1 Photograph of a 100 MeV ^{32}S beam exciting a neon gas target. The cell has a diameter of 100 mm. The beam enters the gas with 200 mbar pressure through a 1.1 mg/cm^2 titanium foil

Excitation processes of gases by energetic ions (e.g., several MeV/amu) can qualitatively be described as follows: The primary projectiles can have a relatively high charge state on the order of + 10e for the Tandem accelerator experiments described here. The ˜ 100 MeV sulfur projectiles travel in the gas together with their remaining electrons. In collisions with the target species, the high charge state and the overlapping electron shells lead to a "violent" excitation of the electron shell of target atoms or molecules (see "Fano Lichten model" [17]). The result is a high probability for excitation and ionization of the target species including the formation of excited ions.

The singly charged secondary electrons formed during the primary ionizing collisions, however, have a low probability for producing excited target ions in single collisions. It can therefore be expected that optical transitions in ionized species are closely related to the primary projectiles, whereas light emission from neutral atoms can also be induced by secondary electrons which may travel long distances depending on their energy and the gas density.

Formation of secondary electrons in heavy ion collisions plays an important role in basic research as well as applications. There is a variety of processes by which secondary electrons are created in ion collisions. Here we just mention that the spectrum of secondary electrons is more concentrated on low energies for ion beam than for electron collisions [18] and falls off exponentially. This component is due to binary collisions. The various components follow the terminology "Delta-electrons" (electrons, which are fast enough to induce further ionization), "cusp-electrons" ("Delta-electrons", traveling with the same velocity as the ions, e.g., [19]), "convoy-electrons" ("cusp" emitted off solids, e.g., [20]), Auger-electrons, etc. They differ in energy and angular distribution. This field of research is also relevant for all kinds of "track-formation" in solids, liquids, and gases [21]. Here we summarize all the electrons which are emitted along the ion path under the term "secondary electrons", and for their contribution to the observed beam profile we are interested in their motion perpendicular to the ion beam axes. We come back briefly to this issue in connection with the beam profiles discussed below. And we want to point out that the profiles, which will be shown below for typically 1 mbar target gas pressure, contain information of the electron energy distribution perpendicular to the beam
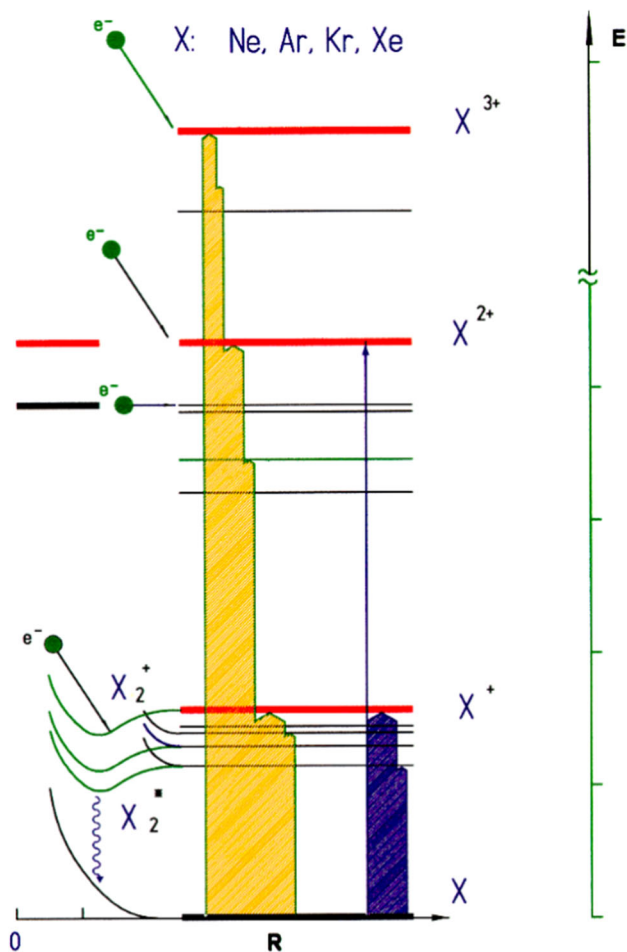

Fig. 2 Schematic representation of excitation processes in rare gases. Here, the red horizontal lines indicate ionization potentials, while the black lines indicate excited levels. The width of the arrows is a semi-quantitative measure of the cross sections for ion excitation (left, yellow) and electron excitation (right, blue). Recombination, charge transfer, and molecule formation are indicated on the left side of the diagram (see also text)

since the 1 mm beam diameter is representative for a single track in comparison with the larger dimensions of the "halo" around the beam. Here, the cross section of secondary electron formation [18] needs to be weighted with the excitation, respectively, ionization cross sections of gases with swift electrons, which are broadly peaked around 100 eV [22]. From the literature cited above, it can be seen that a typical "effective" energy of the secondary electrons is thus ∼50. . . 200 eV for our conditions. This corresponds to a penetration and excitation range of ∼ 1. . . 5 mm in 1 mbar Ne [23]. It will be shown below that this is in good agreement with the dimensions of the halo which we observe.

A schematic scheme of primary and secondary excitation processes is shown in Fig. 2. The figure was prepared for Ref. [24]. It shows a typical arrangement of energy levels of rare gases with the ground state, excited levels, the first ionization energy, excited levels of the

singly ionized target atom, and so on. The width of the left (yellow) arrows is a measure of cross sections for excitation by ion projectiles, and the (blue) arrows on the right represent collisional excitation by (secondary) electrons. The underlying values were taken from literature for the example of argon as target gas. (A detailed discussion is given in [24].) The schematic drawing is meant to explain what has been discussed above, namely that the ion projectiles create excited target atoms also in higher ionization stages in single collisions with significant cross sections. Secondary electrons, however, which have typical maximum energies on the order of 5 keV (and lower) for our example of ∼ 100 MeV sulfur projectiles [25] excite predominantly neutral atoms. Secondary processes proceeding at elevated target densities are sketched on the left side of Fig. 2 (recombination [25], charge transfer [26], excimer molecule formation [12, 27] for which the horizontal axis represents the internuclear distance between two target atoms, and radiative decay of the excimer molecules).

The processes addressed in Fig. 2 are the basis for interpreting our spectroscopic and beam profile data presented below.

2 Experimental setup

The experimental setup consisted of a target cell with a gas system, a scanning monochromator for spectroscopic measurements, and cameras used as a model for beam profile monitors. Details of the setup and sensitivity calibration of the cameras are described in [28].

In brief, a gas target (Fig. 3) was installed at a beamline of the Munich Tandem accelerator. For target gas pressures above 1 mbar the beam entered the target cell through a 1.1 mg/cm^2 Titanium foil. Differential pumping was applied for lower pressures. The beam entered the cell through an aperture of 1 mm diameter. Rare gases to be tested were purified with a gas purifier (MonoTorr PS4-MT3). For pressures above 200 mbar it was circulated through the cell and the gas system. For lower pressures it was extracted as clean gas from a gas cycle and fed into the cell in a continuous flow. The gas system is schematically shown in Fig. 4. A Faraday cup installed at the end of the cell was used for measuring the beam current in the evacuated cell.

Light emitted from the gas target was observed perpendicular to the ion beam axis from one side through a MgF$_2$ window and from the other side through a fused silica window. Spectroscopic measurements were performed with an f = 30 cm scanning monochromator (McPherson model 218) and a phototube (PMT) with MgF$_2$ entrance window operated in counting mode. Light from the beam region was imaged onto the entrance slit of the monochromator by a 1:1 Al-MgF$_2$ mirror optics. This spectroscopic setup can cover a wavelength range from ≈110 nm to 800 nm (1500 nm with an IR-PMT). Sets of filters were used to block higher orders of the spectrum when necessary.
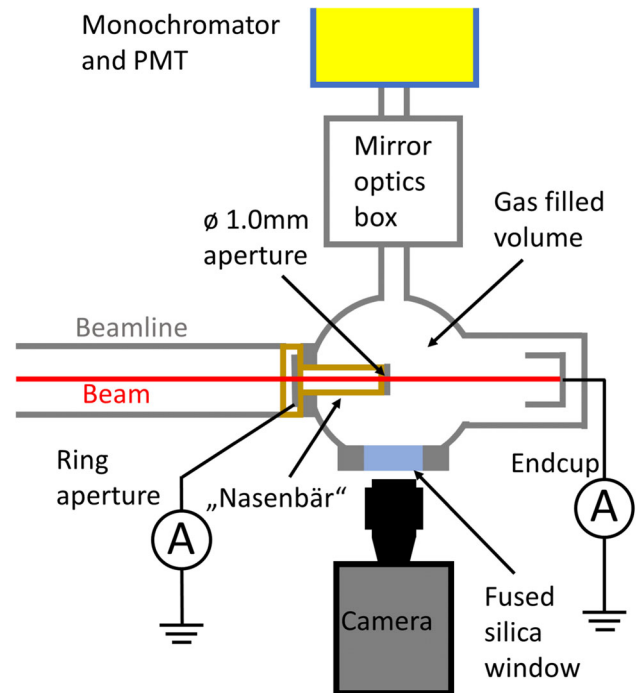

Fig. 3 Schematic drawing of the experimental setup. ("Nasenbär" = coati-mundi, our lab-slang for the beam entrance part)

Three different cameras were tested as beam profile monitors (ATIK 383L + , PI-Max4 1024f, ProEM + 512B). An apochromatic, UV transparent (λ > ∼300nm) lens (Jenoptik UV–VIS-IR 60 mm 1:4 APO Macro) was used to image the beam region through the fused silica window onto the sensitive area of the cameras. Filters were installed in front of the cameras. They were selected according to spectral lines which were found to be of interest in the spectroscopic studies. This study was deliberately limited to a wavelength region from 300 to 800 nm for practical reasons since future beam profile measurements will work with cameras which are easily available and not too expensive. Off-line experiments with a PTB-calibrated tungsten strip lamp (WI 17/G) allowed us to calibrate the sensitivity of the camera systems to determine effective emission cross sections for light emission selected with the filters mentioned above.

In most experiments a continuous 87 MeV (2.7 MeV/u) ^{32}S beam was used as a typical ion beam. A 14 MeV proton beam was used in one of the experiments for comparison. Neon and argon were studied in detail. Other experiments were performed with krypton, xenon and nitrogen as target gas. Two ion beam experiments were prepared with pulsed beams with pulse duration of 320 ns. Time-resolved data were recorded for neon and argon lines.

A special electron beam device (modified E-Lux, Excitech GmbH) was installed and used for recording electron beam-induced spectra for gases identical with those of ion beam excitation. The low-energy electron

Fig. 4 Schematic drawing of the gas system. The red arrows indicate the gas flow for differential pumping and the black arrows the closed cycle when an entrance foil was used for the beam to enter the gas cell
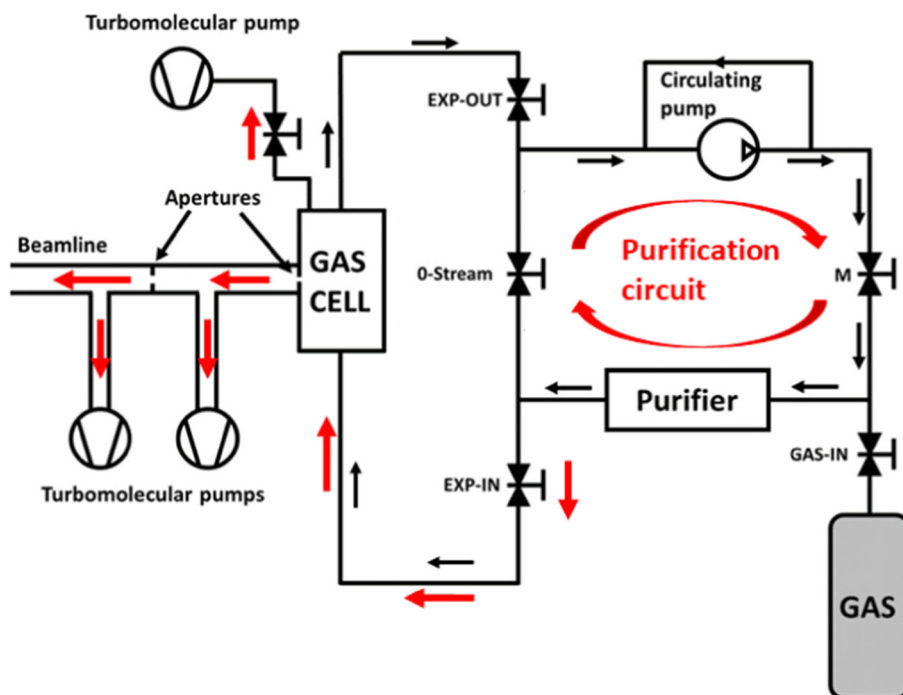
beam excitation technique [12] had been invented to simulate the $< \approx 5$ keV secondary electrons produced in ion beam collisions with ≈ 3 MeV/u sulfur projectiles [25] and is now also used for vacuum ultraviolet excimer light sources (E-Lux, Excitech GmbH). Here, 12 keV electrons are generated in a CRT (cathode ray tube) and exit the tube vacuum into the target gas via a very thin (300 nm) but stable (pressure differential up to several bar) ceramic membrane, resulting in ≈ 10 keV electrons for gas excitation.

3 Spectroscopic results

In the following, results obtained from spectroscopic studies are presented. This allows identification of the emission lines and measuring the target pressure dependence of the intensity of atomic and ionic lines. Effective ion beam-induced light emission cross sections were derived from photographs of the beam in gas targets. A comparison of ion beam and electron beam-induced emission spectra is also given. Then the spatial shape of the light emission obtained with the camera systems is presented and discussed.

3.1 Ion beam-induced pressure-dependent emission spectra of argon and neon

Light emission from argon at a target gas pressure of 600 mbar excited by a 100 MeV sulfur ion beam is shown in Fig. 5. It had been measured in the context of earlier experiments. It shows many of the principal excitation and emission processes discussed for Fig. 2. The second excimer continuum in the vacuum ultraviolet
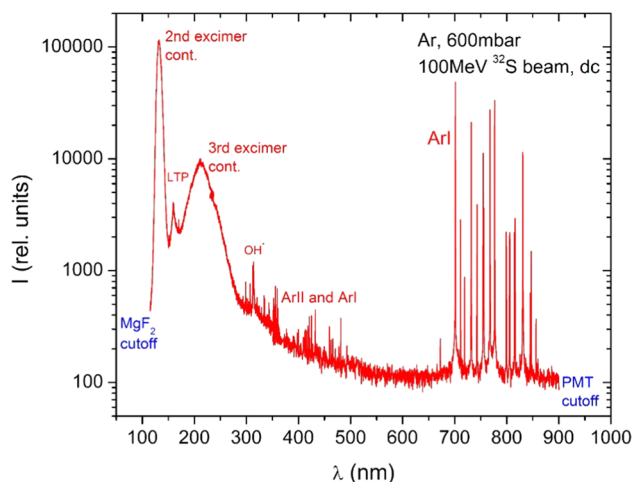
Fig. 5 Overview spectrum emitted from 600 mbar argon excited by a 100 MeV sulfur beam. Molecular (excimer) emission, ionic and atomic lines appear, and an OH^* impurity emission at 310 nm is also visible

spectral region dominates the spectrum (note the logarithmic intensity scale). Toward longer wavelengths it is followed by the classical left turning point (LTP) [29] and the third excimer continuum [30]. The importance of impurities is indicated by the appearance of an OH^* emission at 310 nm [31]. The wavelength region from about 300 to 900 nm relevant for the measurements presented here shows light from optical transitions of ions (ArII) and neutral atoms (ArI).

Optical beam diagnostics is primarily important for observing the beam in a beamline at low pressure of the light emitting gas so that the beam is essentially
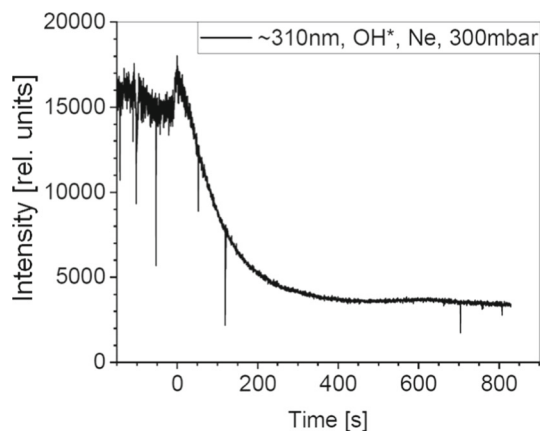
Fig. 6 Effect of gas purification. Stable conditions with respect to gas purity were reached after about 5 min gas circulation/purification. (The short-time high-intensity fluctuations ("kicks") are due to instabilities of the beam current.)

undisturbed by the measurement. There are also target experiments, for example in the field of ion beam-induced plasma physics [32], where it is possible to work with dense gases or even solid state materials. In such a case energy deposition, heating, and expansion has to be considered as a potential modification of the observed beam profile [1]. Here we will show that medium gas densities on the order of 100 mbar are not very sensitive to artificial profile modifications, at least when secondary electrons of an energy of less than about 5 keV are the major contributors to modify the ion beam profile data.

To begin our study, we started with conditions similar to those in Fig. 5 and reduced the target gas pressure step by step. This was motivated by the question of how far down we could go and still get reasonable signals. Experiments with lighter rare gases (i.e., higher excitation energies) were performed before experiments with heavier rare gases to avoid alteration of the spectra due to energy transfer processes: Tiny residues of the heavier gases would be excited due to energy transfer by the bulk light gas. Their emission would show up predominantly, modifying the pure light gas spectra and thus hindering precise measurements.

In a first step, stable conditions with respect to gas purity were ensured. Helium leak tests of the entire system were performed, and 300 mbar of research grade neon 5.0 (99.999%) was filled into the target gas cell. Light emission on the 310 nm OH-transition was monitored over time, as shown in Fig. 6. (from [3]). The main impurity source is water molecules, photo-desorbed from the target cell walls during the experiment, thus randomly contaminating the previously clean gas. Continuous gas purification allows for stable conditions after about 5 min purification time, with continuous, slow improvement over time.

Figure 7 shows a series of argon and neon spectra with reduced target gas pressure. There are two groups of emission lines in both gases, essentially stemming from the respective "Balmer"-like $(n + 1)p \rightarrow (n + 1)s$ transitions. Most of the short wavelength lines are transitions in ionized target species, whereas the longer wavelength lines are the equivalent atomic lines. In the following we will mainly focus on the rare gases neon and argon. Helium has only a few lines while krypton and xenon spectra have too many emission lines of both neutral and ionic lines which cannot be disentangled easily. Furthermore, their high-intensity neutral "Balmer"-lines appear at too long wavelengths to be practical for standard detectors. Nitrogen shows the well-known emission bands of the neutral and ionized molecules between about 300 and 400 nm and 391 nm, respectively [33, 34]. Spectra and beam profiles of Kr, Xe, and N_2 are shown in separate chapters below.

Spectra in Fig. 7 were recorded with the same spectral response, which was not absolutely calibrated, but represents the same intensity ratios between the region of the ion lines in the blue and the atomic lines in the red for all spectra shown. The series of spectra has the main result that there is a significant change in the intensity ratio between ionic and atomic lines with a strong relative increase of the ion lines when the pressure is reduced from 300 to 0.03 mbar or, respectively, a dramatic decrease in intensity of the neutral lines. Several spectra recorded for intermediate pressures were omitted in Fig. 7 for clarity of the figure but were used to determine the pressure dependence of line intensities (Fig. 11).

An interpretation of this result can be found on the basis of the processes indicated in Fig. 2. First, it has to be noted that the absolute intensity of light emission depends of course on the power deposition in the field of view of the spectrometer and this increases with target gas pressure. The most direct process for obtaining light emission is excitation of the target atoms from the ground state into one of the excited levels and a following optical transition, visible in a prompt intensity increase after excitation, and a following exponential decay [10, 35]. Transitions between the levels are not indicated in Fig. 2. Besides optical transitions, there are collisional de-excitation processes induced by collisions with target atoms or free electrons (quenching). Since the gas is weakly ionized, collisions with ground state atoms play the dominant role. This collision rate decreases with decreasing target gas pressure. This change in the branching ratio between optical and collisional de-excitation with decreasing pressure favors the optical transitions which helps to get reasonable optical signals down to low pressures. A quantitative discussion on this effect will be given below for the case of the pressure dependence of ion lines.

If direct excitation from the ground state into excited states would be the only light producing mechanism the changing intensity ratio with varying pressure could not be explained. We interpret the dominance of the atomic lines at elevated target gas density by two effects: First, higher energetic secondary electrons produced in the primary collisions can lead to additional excitation processes, and this, according to Fig. 2, predominantly

Fig. 7 Overview spectra of argon and neon at different target gas pressures. (Please note that for some spectra (Ar, Ne 300 mbar, Ne 0.03 mbar) we did not record "empty" spectral regions, simply in order to safe accelerator time)
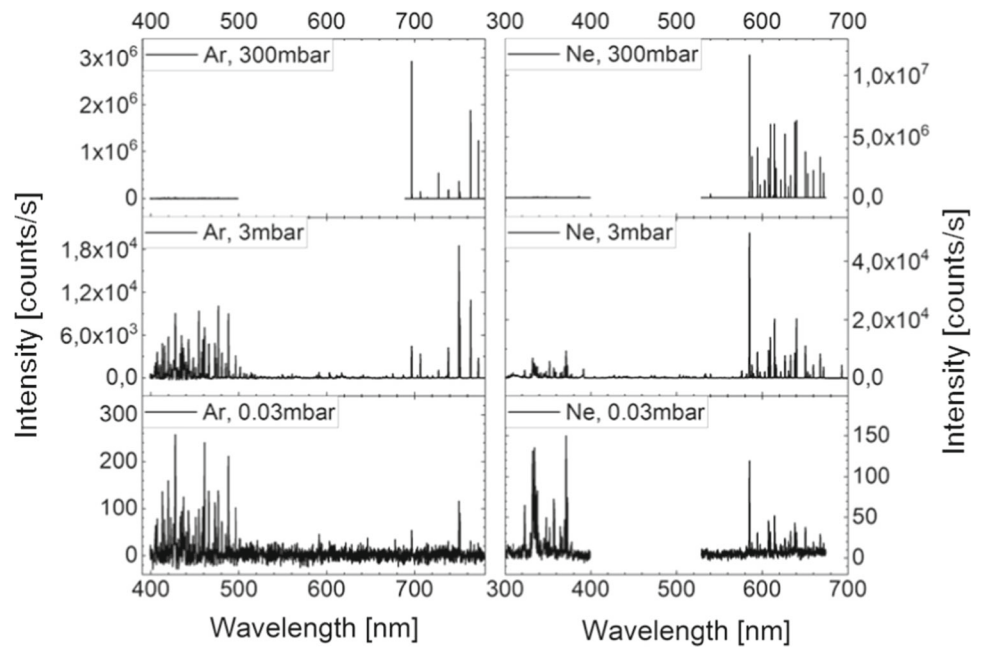
into excited states of neutral atoms. Second, the secondary electrons will cool down and finally recombine with ions, populating excited levels [25, 36–38]. Since singly ionized target species have a higher density than multiple-ionized ions, recombination plays a major role from singly ionized species into excited states of neutral atoms. The subsequent optical transitions then contribute to the observed optical signal. How much recombination contributes to the emission will be demonstrated by time-resolved measurements described below.

In summary, it is particularly interesting to study ionic emission lines at low target gas pressure for ion beam diagnostic applications, as already suggested by the mechanisms sketched in Fig. 2.

In Fig. 8 emission spectra of argon and neon are plotted for a target gas pressure of 0.3 mbar for comparison. This shows that argon can be used for beam diagnostics preferentially between 400 and 500 and neon between 300 and 400 nm. The wavelength resolution in Fig. 8 is 0.6 nm (200 μm slit width of the monochromator). An example of spectra recorded with 0.06 nm resolution is shown in Fig. 9. It demonstrates that individual lines could be observed separately and clearly identified.

The spectral results allowed to identify lines. Lines were then selected with filters in space-resolved measurements using the cameras mentioned in the Sect. 2, "experimental setup" above. An example of a spectrum with a filter curve is shown in Fig. 10 for mainly selecting the 585.25 and 589.19 nm atomic lines in neon.

Integral intensity values of selected ion- and atomic lines with higher intensity were derived from the series of spectra at different target gas pressures of argon. These values are plotted in Fig. 11. The atomic lines show a continuous, essentially linear intensity increase on a double-logarithmic scale. About four decades in pressure were covered with this spectroscopic setup.
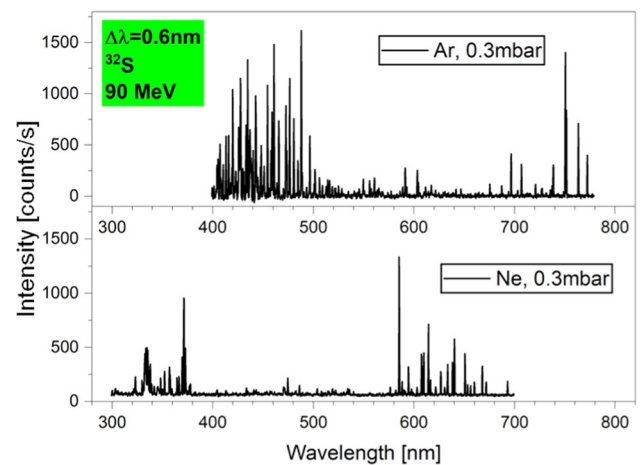
Fig. 8 Ion beam-induced emission spectra of argon and neon at a relatively low pressure of 0.3 mbar are shown. Particularly, the ion lines between 400 and 500 nm in argon are suggested as useful lines for beam profile measurements

The intensities of the ionic lines significantly bend off toward higher target density. We interpret this behavior by collisional de-excitation. The intensities of the atomic lines show a continuous increase with pressure (gas density), with partly more than linear behavior at some lines, which is particularly visible at the Ar I, 696.5 nm line (green curve in Fig. 11). We interpret this by excitation also by secondary electrons and recombination as discussed above.

For selected lines, we studied the intensity-vs-pressure behavior to very low gas densities, as shown in Fig. 11, lower panel. Here, two of the most intensive atomic (585 nm) and ionic (337 nm) Neon lines are presented, with the intensity given in absolute units.
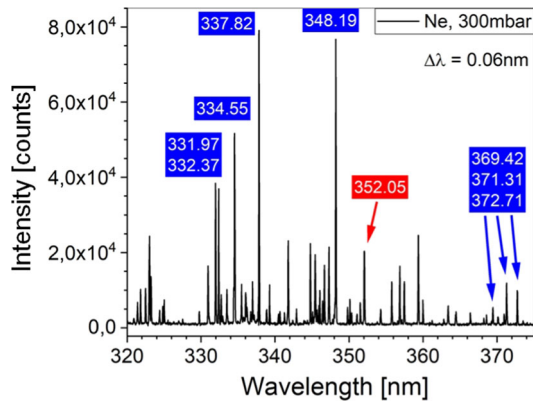
Fig. 9 Expanded view of a neon emission spectrum with 0.06 nm wavelength resolution. The lines could be clearly identified as demonstrated for a selected sample of lines. Ion lines are indicated in blue and an atomic line in this region in red
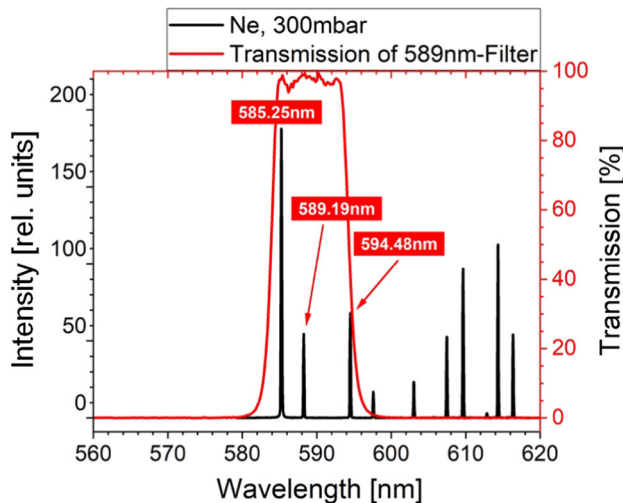

Fig. 10 Emission spectrum of neon plotted together with a filter curve to select three atomic lines for the space-resolved studies with the cameras for beam profile diagnostics

Fig. 11 Intensities of selected atomic and ionic lines versus pressure for argon (relative units, Ar I (atomic) and Ar II (ionic), upper panel), respectively neon (absolute emission rates, atomic line: red circles, ionic line: blue squares), lower panel. Collisional quenching is readily observed for the ionic lines in both argon and neon (see also text for an interpretation). Examples of the pressure dependence to very low values are shown in the lower panel

Again, a positive slope (super-linear increase in intensity) can be seen for the atomic line at higher pressures, indicating contribution of secondary processes playing a prominent role, while quenching processes diminish the intensity of the ionic line significantly.

In order to study if, and how much, in particular recombination plays a role in the excitation process for the atomic lines, we have pulsed the ion beam, set the monochromator to the 696.5 nm line of argon and recorded time-resolved light emission data (Fig. 12). The result is similar to the one obtained for excimer emission studied in Ref. [25]. There we had modeled the time spectra to obtain time dependent electron densities and electron temperature in the ion beam-induced plasma. The delayed increase of intensity in recombination-driven light emission is explained by
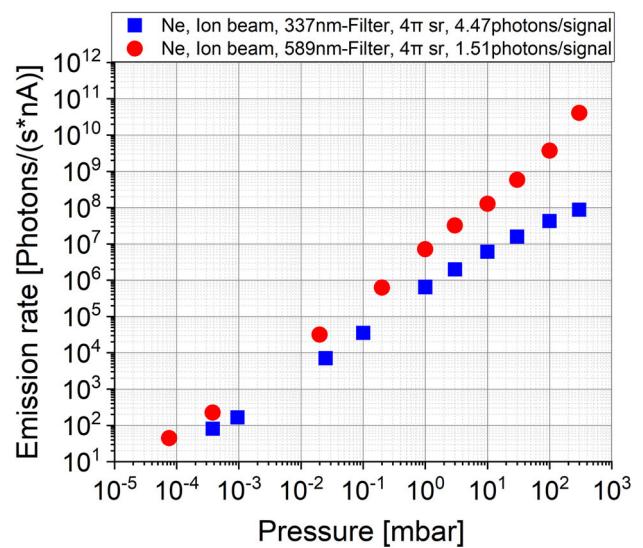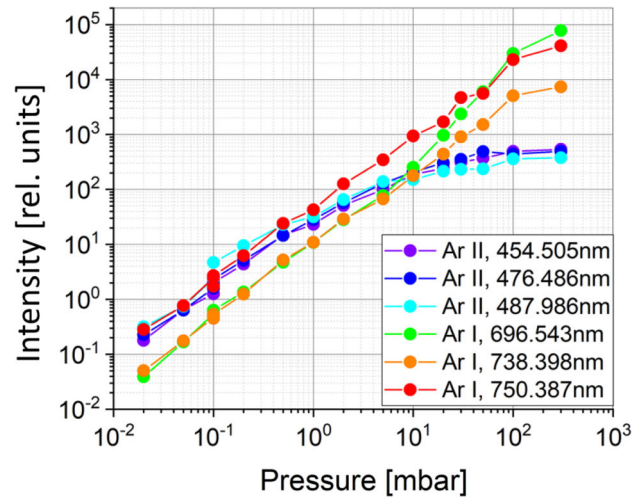
cooling of the electrons following their primary production with up to keV energies. A delayed onset of emission (laser effect) was also observed for ion beam-pumped recombination lasers [14, Fig. 9 therein]. Some recombination from higher ionization (ArIII and higher) contributes also to the emission of the 476.5 nm line of ArII but only at high pressures and at a significantly lower level (Fig. 12 lower panel).

The upper levels of the ionic lines are predominantly directly excited in primary collisions and increasingly quenched by collisions with target atoms at elevated density in competition with the optical transitions (no cascades, recombination, and molecule formation assumed). Note, the excitation energy of the
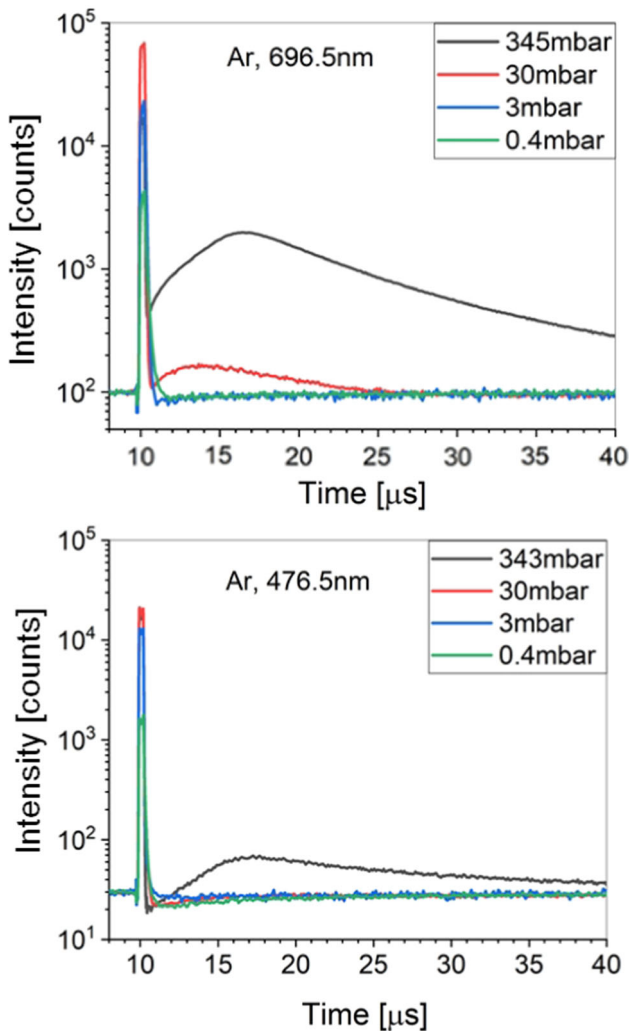
Fig. 12 Time spectra recorded for an atomic ("neutral")(top) and an ionic (below) line of argon. The delayed emission is due to transitions following recombination (see also text)

observed lines is larger than the ionization potential of the respective neutral atoms. Any collision between a neutral atom and an excited ionic species thus usually results in a quenching process of the excited level by ionizing the neutral collision partner. This process can be described by a direct population rate σNj and depopulation by the optical and collisional transitions:

$$dN^*/dt = \sigma Nj - N^* A_{ik} - k_q N N^*. \qquad (1)$$

Thereby N^* is the population density of the upper level, σ the excitation cross section, N the target density, j the flux density of the ion beam, A_{ik} the optical transition rate, and k_q the rate constant for collisional quenching (to be determined in the following way). For a constant ion beam flux we have equilibrium conditions and thus $dN^*/dt = 0$.

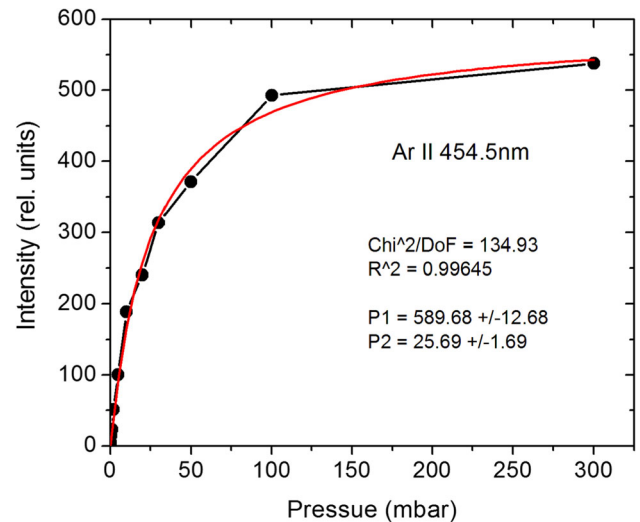$$0 = \sigma Nj - N^* A_{ik} - k_q N N^* \text{ and thus} \qquad (2)$$

Fig. 13 Intensity of the 454.5 nm ArII line (see also Fig. 10) plotted with a linear intensity scale and fitted by Eq. (5). The fit results in P2 = 25.7 ± 1.7 mbar

$$N^* = \sigma Nj/(A_{ik} + k_q N). \qquad (3)$$

This leads to a formula for the intensity I ($\sim A_{ik} N^*$) of the ion lines versus the measured pressure p:

$$I(p) \sim I(N) \sim A_{ik} N^* = A_{ik} \sigma Nj/(A_{ik} + k_q N) \qquad (4)$$

Introducing two fit parameters P1 and P2, (4) can be rewritten with N proportional to pressure p and dividing numerator and denominator by k_q N to:

$$I(p) = P1/(1 + P2/p). \qquad (5)$$

Here, P1 represents a relative intensity proportional to the ratio between light emission and quenching ($\sim A_{ik}/k_q$), while P2 represents the ratio between light emission and quenching, normalized to the particle density N at pressure p: $P2 = A_{ik} / k_q * p/N$, essentially indicating the pressure where the quenching rate $k_q *N$ equals the optical transition rate A_{ik}.

N can be converted into p by $N/p = 2.7 \times 10^{16}/(cm^3$ mbar) for normal conditions. Then:

$$k_q = A_{ik}/(P2 * 2.7 \times 10^{16}/mbar\ cm^3). \qquad (6)$$

An example is shown in Fig. 13 for the analysis of the 454.5 nm $(4p^2P_{3/2}°—4s^2P_{3/2})$ ArII line.

Equation (6) provides a collisional rate constant $k_q = (6.8 \pm 0.4) \times 10^{-11}$ cm^3/s, based on a tabulated A_{ik} value of 0.47×10^8 /s [39]. The three Ar-ion lines which have been measured showed collisional rate constants between ≈ 1.5 and 7×10^{-11} cm^3/s. This corresponds to collision cross section σ_c on the order of 10^{-15} cm^2 and collision radii of 10^{-8} cm (v = 300 m/s thermal speed and $< \sigma_c v > = k_q \approx 3 \times 10^{-11}$ cm^3/s) in good agreement with atomic dimensions.
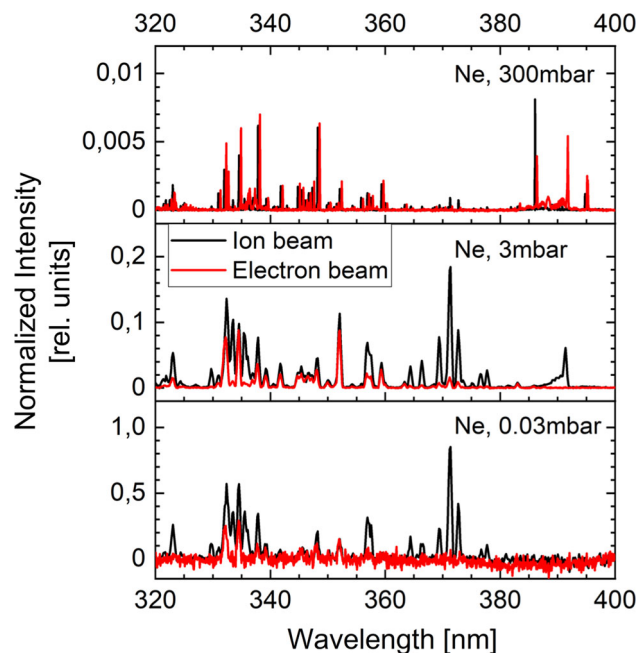
Fig. 14 Comparison of ion beam (black) and electron beam (red, slightly shifted to the red for clarity)-induced spectra in the region of ion lines of neon. At higher gas densities the spectra are very similar. At low pressure the ion lines are almost entirely excited by the heavy ions only. Please note that the depicted intensity values are normalized to the target gas pressure (i.e., density)

3.2 Comparison of ion beam with electron beam-induced spectra

A technique, indeed originally invented for comparing the primary ion-projectile and secondary electron excitation, was used to study the difference between ion beam and electron beam-induced spectra in the sense of Fig. 2. Low energy electron beam excitation simulates the secondary electrons [12]. The technique has meanwhile been widely used for electron beam-driven vacuum ultraviolet light sources and their applications [40].

A comparison of ion- and electron beam-induced spectra for identical gas targets is shown in Fig. 14. This clearly demonstrates the predicted behavior that ion beam excitation at elevated gas density occurs mainly via secondary electrons (very similar spectra). At low-target gas density the ion lines are only excited by the heavy projectiles.

3.3 Spectra of krypton, xenon, and nitrogen

In this chapter we very briefly discuss some aspects of the emission from species for which we have recorded a more limited amount of data. For the case of krypton, Fig. 15 demonstrates that neutral (KrI) and ionic (KrII) lines appear in the same spectral region with similar intensities. This would make an application for beam

profile measurements with optical filters more complicated than for neon and argon where the neutral and ionic lines form separate bunches. Krypton thus has not been investigated any further.

Only one spectrum has been recorded for xenon (Fig. 16). Besides a vast amount of only weak lines, there is a distinct underlying continuum visible. Since there was no obvious bright, doubtlessly identifiable, and with optical filters easily separable structure recognizable, xenon has been (for the time being) discarded as a promising target for beam profile measurements, and has not been studied within the framework of this project.

Nitrogen may be of interest for beam profile measurements. It has been studied by P. Forck and F. Becker in more detail [16]. In Fig. 17 we show nitrogen spectra for target gas pressures between 0.1 and 15 mbar. As in the case of neon and argon lines, the neutral lines appear with reduced intensity at reduced target gas pressure. For nitrogen the effect is especially pronounced because the neutral emission bands of nitrogen (C → B, so-called second positive system) start at a level (C) which is not connected with the ground state by an allowed transition. Electron beams can drive this transition more easily than heavy ion projectiles. This discrepancy will become even more pronounced for the beam profiles, as will be discussed below

4 Ion beam profile measurements

A ^{32}S ion beam from the Munich Tandem accelerator was sent through a 1 mm diameter aperture into the target cell. Since the last magnetic quadrupole doublet has a long focal length of about 4 m it could be assumed that the beam has the same 1 mm diameter at the point of observation a short distance behind the entrance aperture. We assume that scattering off the rim of the aperture and angular scattering in the entrance foil (when used) and the few cm of gas do not influence the beam shape noticeably. Therefore, the profiles are a measure of the quality of the profile monitor.

The three cameras (ATIK 383L + , PI-Max4 1024f, ProEM + 512B), always equipped with the same apochromatic lens, were used to take pictures of the beam-induced light emission. An example of the raw data is shown in Fig. 18. Note that while low energy electron beams do not form collimated beams, the shape of the excited volume can nevertheless also be studied with similar optical methods [41].

4.1 Ion beam profile measurements in neon and argon

Assuming optically thin plasma, the data from Fig. 18 represent a projection of the beam-induced light into the detector plane. Defining a region of interest perpendicular to the ion beam axis leads to data like those

Fig. 15 Pressure series of ion beam excited Krypton. Ionic and neutral lines appear with comparable intensities closely spaced. Please note that—for comparison—all spectra are normalized to the 431.9 nm line peak
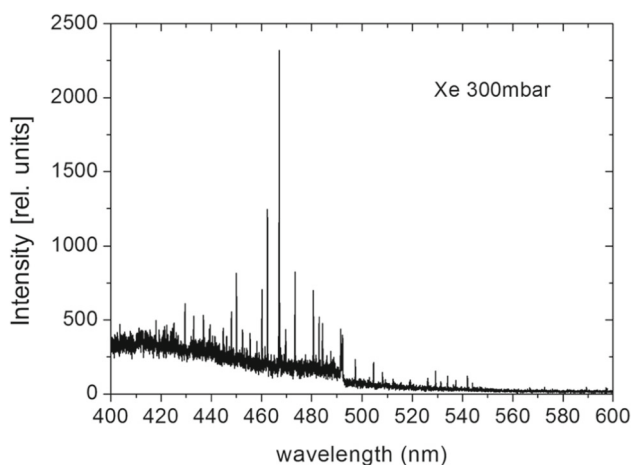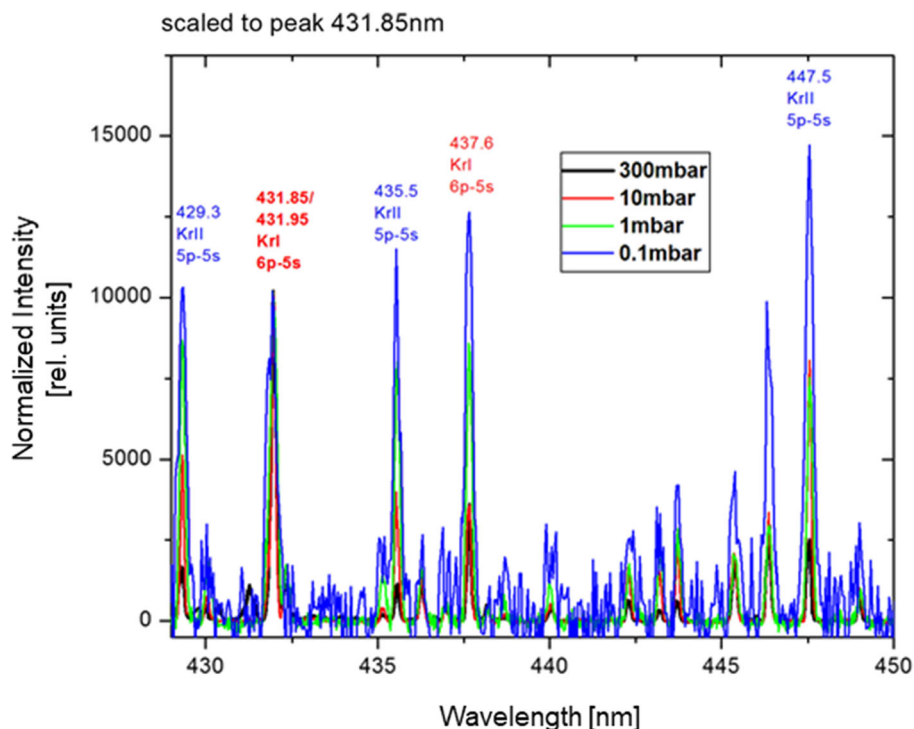

Fig. 16 A heavy ion beam-excited 300 mbar xenon spectrum in the visible range between 400 and 600 nm is shown. Relatively weak lines additionally to an underlying weak continuum are present

shown in Figs. 19 and 20. These figures show the projected beam profiles for neon and argon over a wide pressure range and for the ion- and atomic lines selected by the appropriate filters. Whereas the ionic lines indicate always essentially the same profile, the atomic lines show a profile which widens up going from high pressure target gas to lower pressure and becomes narrower again toward even lower pressure. This can easily be understood in connection with the discussion of Fig. 2. The broad wings appearing for the atomic lines at pressures around 1 mbar are caused by secondary electrons which can strongly excite the atomic lines in

single collisions but not those of excited target ions. At higher pressures like the 50 and 100 mbar data shown in Figs. 19 and 20 the range of the secondary electrons is so short that excitation by the electrons occurs "locally", i.e., well within the 1 mm beam diameter. For low target gas pressures the range of the secondary electrons is very large in comparison with the ion beam diameter so that excitation around the ion beam, modifying the profile, can be neglected.

A quantitative study of track radii of ion beams has recently been performed for liquid argon in the context of particle detectors [21]. A key information in that study is that 66% of the energy deposited by an ion beam in liquid argon is confined in an inner core of about 10 nm diameter around the ion path. A conversion to 1 mbar in the gas phase leads to ~12mm radius for the inner core, consistent with the dimensions observed here for the atomic lines. (Please note that a major part of the ion beam produced energy deposition in a target stems from secondary electrons!).

We have so far used "beam profile" as "projected beam profile". In cases where a "real" *radial* beam profile j(r) has to be known, data from the projected light intensity measurements can be converted to radial profiles when assumptions of low optical density and azimuthal symmetry of the beam are valid. The conversion is achieved by Abel inversion of the data for the "projected profiles". An example is shown in Fig. 21. The radial profile obtained by Abel inversion is significantly narrower than the projected profile. This can be understood by some simple, but not trivial, geometrical considerations.

Fig. 17 Comparison of neutral (black) and ionic (blue) nitrogen emission, using heavy ion beam excitation, at different pressures. At higher gas densities the spectrum is dominated in this spectral range by the C-B, 0–1 transition of neutral nitrogen. At low pressure the neutral lines are almost absent, due to the sole excitation by secondary electrons, while the ionic B-X emission (391 nm) is entirely excited by the heavy ions only and stays constant with the pressure normalized intensity
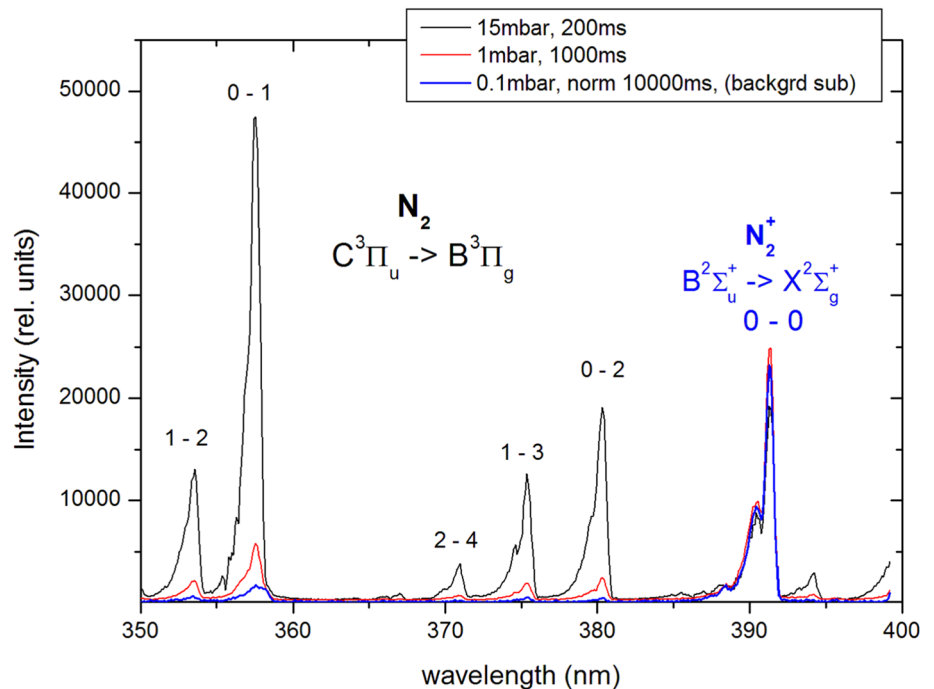

Fig. 18 Sulfur ion beam interacting with a 1 mbar argon gas target. This photograph was recorded with an ATIK383L + camera through a 740 nm Filter and the lens described in the text

4.2 Beam profile of molecular nitrogen emissions

A comparison of beam profiles recorded through filters for 337 nm (neutral nitrogen molecules, C–B, $v =$ 0–0 transition) and 391 nm (ionized nitrogen molecules, B–X transition) shows an interesting effect: The selection rules allow only the secondary electrons to excite the neutral C-states leading to the emission of 337 nm N_2 (C $\rightarrow$ B) light, with no contribution of direct excitation by heavy ions (Fig. 22); thus, no central core is visible. On the other hand, and as with ionic line emission in, e.g., argon or neon, heavy ions strongly excite the ionic N_2 ($B^2\Sigma_u^+$) level, with some additional contribution of energetic electrons, as seen in the wings of the profile.

5 Effective excitation cross sections

Beam profile measurements are necessary in electron and heavy ion beam accelerators. We hope that this study, together with qualified estimates for the individual situation, can help to predict the achievable signal to noise ratio and the required exposure times for future beam diagnostics. Therefore, we have measured typical effective excitation cross sections of light emission for the present data obtained with the ^{32}S beam. "Effective" means that we have not tried to disentangle the processes discussed above and in connection with Fig. 2.

The measurements were performed using the ATIK 383L + , ProEM + , and PIMax-4 camera systems, as typical representatives of a non-intensified CCD, a so called "electron multiplier CCD", and an MCP-intensified CCD camera, respectively. Light from different optical transitions was selected by using filters. Cross sections for individual lines can be estimated from the intensity ratios of the spectral lines.

Absolute intensity measurements are often difficult. Here we have calibrated the sensitivity of the lens-camera systems, using pictures recorded of an absolutely calibrated tungsten strip lamp (OSRAM Wi17/G with calibration data sheet). The calibration technique is described in detail in Ref. [28]. The result for the filter-selected ionic and atomic lines of argon and neon are shown in Figs. 23 and 24, respectively. Regions where the titanium entrance foil for the ion beam was used and regions with differential pumping are indicated. The results show again additional population processes for the atomic lines at elevated pressures and collisional quenching, predominantly of the ion lines, above a pressure of about 1 mbar. Values for the lowest pressures can be interpreted as being valid for cross
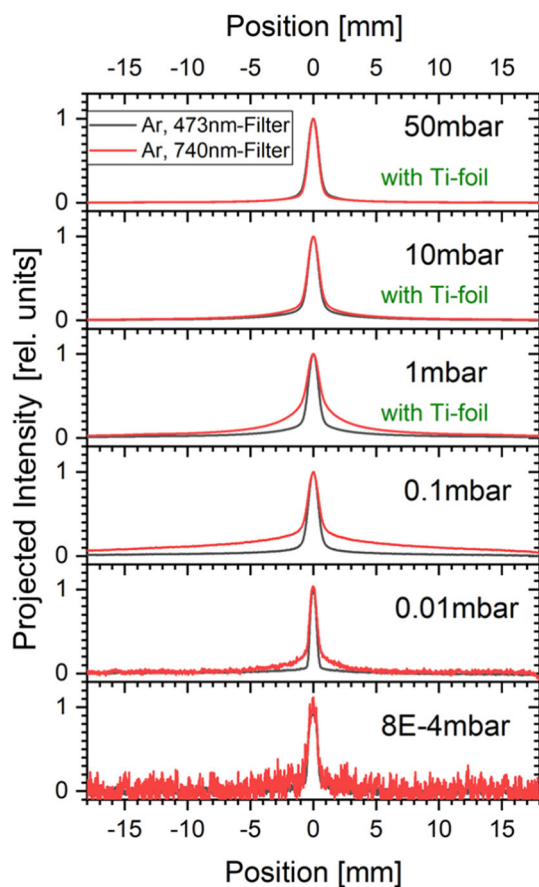
Fig. 19 Beam profiles recorded for argon at different target gas pressures. Projected intensity values derived directly from the raw data are shown, demonstrating the difference in spatial distribution of atomic lines (red) versus ionic lines (black). The widening for pressures around 1 mbar for the atomic lines is due to secondary electrons as explained in the text

Fig. 20 Beam profiles recorded for neon at different target gas pressures. Projected intensity values derived directly from the raw data are shown. The widening for pressures around 1 mbar for the atomic lines (red curve) versus ionic lines (black curve) is explained in the text

sections for direct excitation of the upper level of the optical transition in question—may be with some feeding from higher lying levels – without contribution of recombination or excitation by secondary electrons.

A detailed description of the cross section measurement is given in Ref. [3]. In short, light emitted from the ion beam excited plasma is wavelength-selected by optical filters. An intensity-calibrated lens-camera optical system, as described above, has been used to record the beam-induced light emission. The recorded light signal was integrated over a defined region of interest, and the according beam volume element has been determined by measuring the magnification-ratio of the lens-camera system. Absolute (electrical) ion beam current was measured prior to data-taking in the evacuated gas cell, using a calibrated end-cup with 100 V suppressor voltage applied. Relative beam intensities were recorded during measurements. Cross sections were normalized to *particle* beam currents, using the accelerator-selected
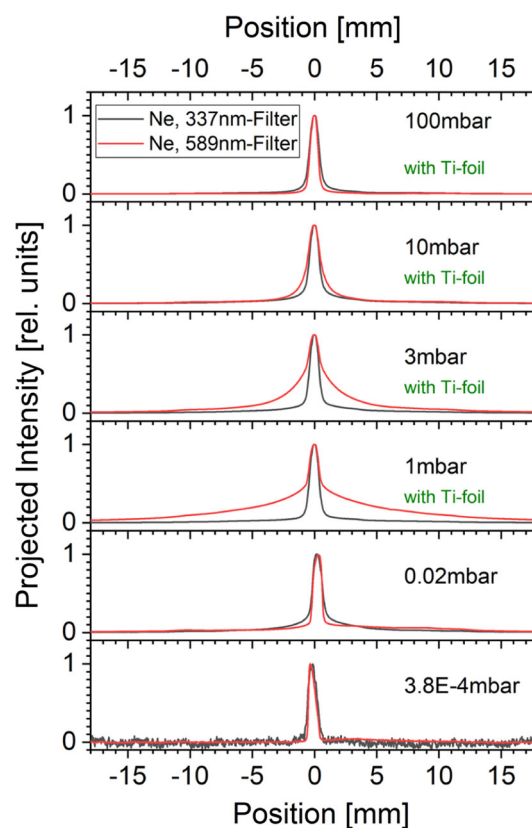
ion charge (8 + , respectively 10 + for some measurements) in case of differential pumping and no additional entrance foil applied, and 13.5 + , the equilibrium charge state for 2.7 MeV/u S-ions [42], in case the Ti-entrance foil was used and the selected 8 + beam-ions were further ionized. A jump in the emission cross section, due to higher charge and thus higher specific stopping power of a single ion, can be seen at the pressure where both, differential pumping and entrance foil data were used (Figs. 23, 24).

Effective optical excitation cross sections then have been derived by:

$$\sigma = \frac{\text{number of emitted photons}}{I * t} * \frac{q * A}{N}$$

Here $A = \pi \cdot (0.5 \text{ mm})^2 = 0.785 \text{mm}^2$ is the cross-sectional area of the beam. N is the number of target particles in the volume $V = A \cdot l_{\text{Pixel}}$, with the pixel width l_{Pixel}, the width of the image of a pixel at the position of the beam.

The charge of the ions is q, the electrical beam current is I and the exposure time is t. Error bars indicate the statistical errors and include systematic errors as
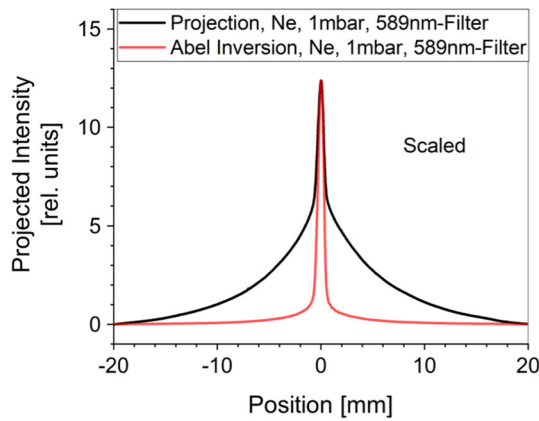
Fig. 21 Example of an Abel inversion of a projected profile (black, wide) into a radial profile (red, narrow). Interestingly there is a large difference. The Abel-inverted profile is much narrower than the profile obtained from the raw data
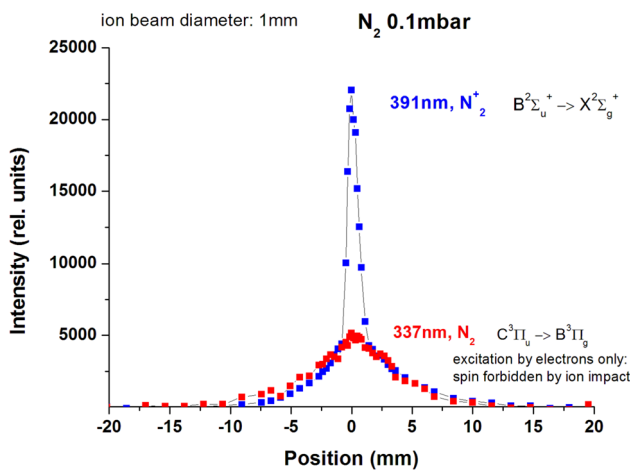

Fig. 22 Measured projected beam profiles of 0.1 mbar nitrogen, excited by a 1 mm diameter ^{32}S-beam. In the profile, measured via the 391 nm ionic nitrogen transition, a "beam-core", as well as a secondary electron-induced halo is visible. In the 337 nm (neutral) profile, only the electron halo is represented, since the heavy ions cannot excite the 337 nm upper level

Fig. 23 Effective (see text for explanation) cross sections at various gas pressures for the ionic (blue, mainly 476.5 nm) and atomic (red, mainly 738.4 nm) argon lines, indicated. Please note the different ranges for "Differential pumping" and "Ti entry-foil" in the atomic (red, upper) and ionic (blue, lower indication) data set, respectively, explaining the difference in the emission cross section "jump" due to different charge states of the projectile

Fig. 24 Effective (see text for explanation) cross sections at various gas pressures for the ionic (blue, mainly 337.8 nm) and atomic (red, mainly 585.2 nm) neon lines indicated

far as they could be measured. Please note that multiple "beam times" have been used to receive the data, with each time setting up the accelerator from anew. The consistency of the data, as well as rare outlier data (e.g., value for Ar-740 nm, 6×10^{-4} mbar), indicates thus the overall reproducibility of the total setup.

Due to the spectrally wide separation of the neutral (atomic) and ionic $(n + 1)p \rightarrow (n + 1)s$ transitions in neon and argon, the respective multiplets can easily be separated by filters and observed as one entity (indicated in Fig. 25 as "ionic fraction", respectively "neutral fraction"). This would give essentially an order of magnitude more light, compared to the observation of single lines, as shown in Fig. 25, without compromising too much on the specifics of ionic or neutral transitions.
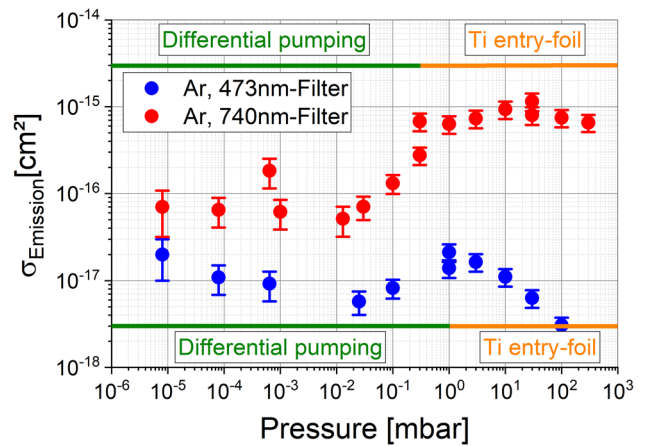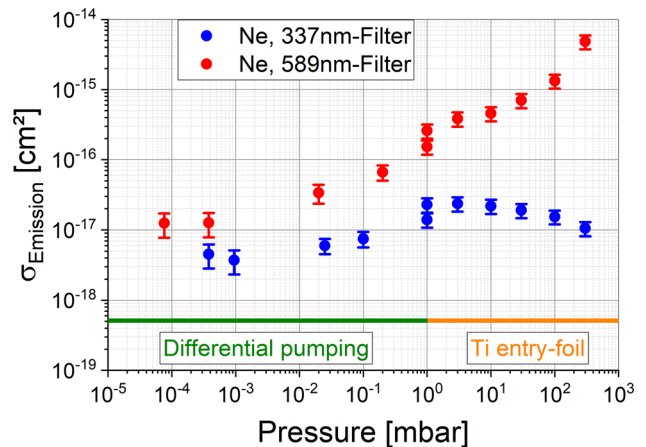
A slightly different behavior of excitation and quenching is represented by nitrogen: Here, the absolute excitation energy of the ionic B-state is not sufficient to ionize neutral nitrogen molecules in energy transfer collisions. Thus, the apparent emission cross section for the N_2^+ 391 nm emission is essentially constant over the entire observed pressure range, since no quenching takes place. Correspondingly, the cross section for the neutral nitrogen 337 nm-band emission decreases continuously with decreasing pressure, as shown in Fig. 26. Here, only secondary electrons contribute to the upper C-level excitation; they escape more and more from the
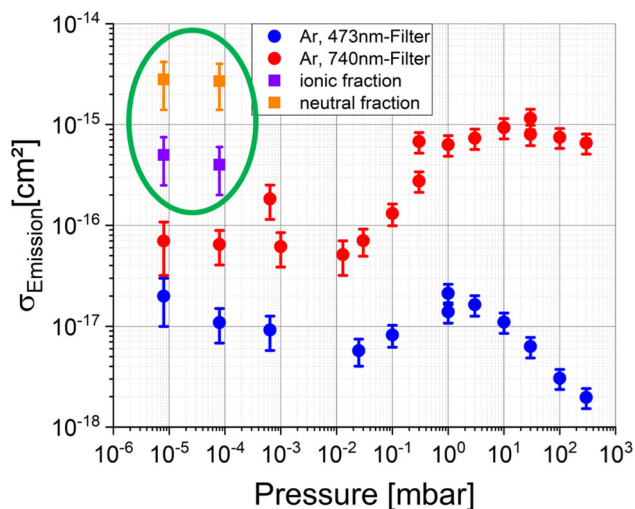
Fig. 25 Effective (see text for explanation) cross sections at various gas pressures for the two argon bands, indicated. Additionally shown are the effective emission cross sections of the total 4p emission multiplet of the ionic and neutral argon states (from [3])
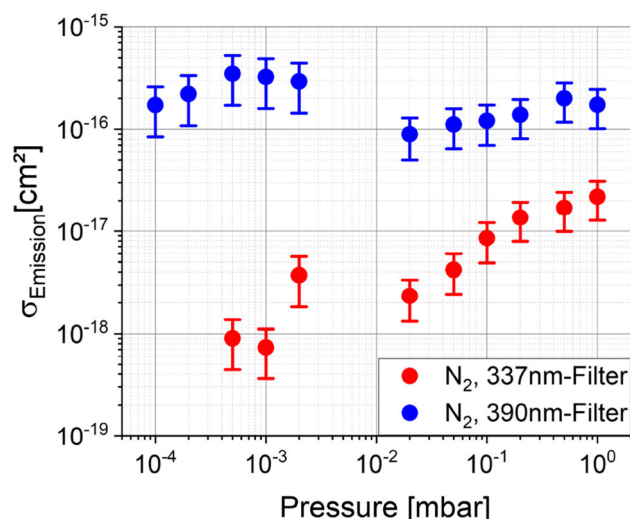

Fig. 26 Effective (see text for explanation) cross sections at various gas pressures for the two nitrogen bands indicated (from [3])

observed volume with decreasing pressure. No 337 nm-nitrogen emission could reasonably be detected below 5×10^{-4} mbar target pressure.

For scaling purposes, one set of data has been measured, using a 14 MeV proton beam. Here, only a relatively low beam intensity of ~ 5nA was allowed because of radiation protection regulations. Thus, the minimum pressure for any reasonable signal was 10^{-3} mbar in case of the 585 nm Neon line (Fig. 27). However, as can be seen in Figs. 23, 24, 25, no large modifications of the cross sections due to secondary effects are to be expected below this pressure range.
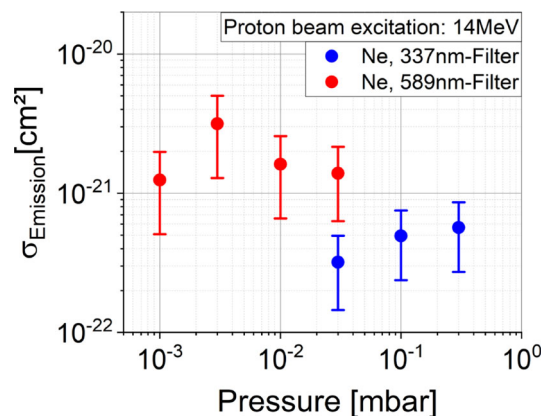

Fig. 27 Effective (see text for explanation) cross sections at various gas pressures for the ionic (blue) and neutral (red) neon line bands indicated, excited by a 14 MeV proton beam (from [3])

Author contribution

All authors contributed equally to the paper.

Data Availability Statement This manuscript has associated data in a data repository. [Authors' comment: The datasets used and/or analyzed during the current study are available from the corresponding author on reasonable request].

Declarations

Conflict of interest The authors declare that they have no Conflict of interest.

References

1. D. Varentsov, A.D. Fertman, V.I. Turtikov, A. Ulrich, J. Wieser, V.E. Fortov, A.A. Golubev, D.H.H. Hoffmann, A. Hug, M. Kulish, V. Mintsev, P.A. Ni, D. Nikolaev, BYu. Sharkov, N. Shilkin, V.Y. Ternovoi, S. Udrea, Transverse optical diagnostics for intense focused heavy ion beams. Contrib. Plasma Phys. **48**, 586 (2008). https://doi.org/10.1002/ctpp.200810092

2. T. Tsang, "A New Luminescence Beam Profile Monitor for Intense Proton and Heavy Ion Beams" Brookhaven National Laboratory, Report No. BNL-81860-2008-IR (2008)

3. R. Hampf, Dissertation, TU-München, (2022). https://mediatum.ub.tum.de/603821?query=hampf&show_id=1537848&srcnodeid=603821

4. F. Becker, P. Forck, T. Giacomini, R. Haseitl, B. Walasek-Hoehne, F.M. Bieniosek, P.A. Ni, D.H.H. Hoffmann, Beam induced fluorescence monitor - Spectroscopy in Nitrogen, Helium, Argon, Krypton and Xenon gas, Proceedings of BIW10, TUPSM020 (2010). https://accelconf.web.cern.ch/BIW2010/papers/tupsm020.pdf

5. A. Ulrich, H. Bohn, P. Kienle, G.J. Perlow, Heavy ion beam pumped He-Ar laser. Appl. Phys. Lett. **42**, 782–784 (1983). https://doi.org/10.1063/1.94086

6. A. Ulrich, J.W. Hammer, W. Biermayer, Lasers pumped by ion beams. J. Appl. Phys. **63**, 2206 (1988). https://doi.org/10.1063/1.341087

7. B. Busch, A. Ulrich, W. Krötz, G. Ribitzki, J. Wieser, Heavy ion beam pumped amplified spontaneous emission on the 172 nm xenon excimer transition. J. Appl. Phys. **74**, 5960 (1993). https://doi.org/10.1063/1.355208

8. A. Ulrich, J. Wieser, R. Pfaffenberger, B. Busch, W. Krötz, H.-J. Körner, G. Ribitzki, Murnuick, optical gain on the 476.5 nm Argon-ion laser line in a gas-target excited by a heavy ion beam. Z. Phys. A **341**, 111 (1991)

9. A. Ulrich, A. Adonin, J. Jacoby, V. Turtikov, D. Fernengel, A. Fertman, A. Golubev, D.H.H. Hoffmann, A. Hug, R. Krücken, M. Kulish, J. Menzel, A. Morozov, P. Ni, D.N. Nikolaev, N.S. Shilkin, V.Y. Ternovoi, S. Udrea, D. Varentsov, J. Wieser, Excimer laser pumped by an intense, high-energy heavy-ion beam. Phys. Rev. Lett. **97**, 153901 (2006). https://doi.org/10.1103/PhysRevLett.97.153901

10. A. Ulrich, B. Busch, W. Krötz, G. Ribitzki, J. Wieser, D.E. Murnick, Emission of light from matter excited by heavy-ion beams. Nucl. Instr. Method A **278**, 72 (1989). https://doi.org/10.1016/0168-9002(89)91133-9

11. G. Ribitzki, A. Ulrich, B. Busch, W. Krötz, R. Miller, J. Wieser, Heavy ion beam excitation of rare gases. Z. Phys. D **21**, 169 (1991). https://doi.org/10.1007/BF01426278

12. J. Wieser, D.E. Murnick, A. Ulrich, Vacuum ultraviolet rare gas excimer light source. Rev. Sci. Inst. **68**, 1360 (1987)

13. J. Wieser, M. Salvermoser, L.H. Shaw, A. Ulrich, D.E. Murnick, H. Dahi, Lyman-alpha emission via resonant energy transfer. J. Phys. B **31**, 4589 (1998). https://doi.org/10.1088/0953-4075/31/20/017

14. C. Skrobol, T. Heindl, R. Krücken, A. Morozov, R. Steinhübl, J. Wieser, A. Ulrich, A miniature electron beam pumped laser. Eur. Phys. J. D **54**, 103 (2009). https://doi.org/10.1140/epjd/e2009-00175-8

15. T. Dandl, H. Hagn, T. Heindl, R. Krücken, J. Wieser, A. Ulrich, Electron-beam–ignited, high-frequency–driven vacuum ultraviolet excimer light source. EPL **94**, 53001 (2011). https://doi.org/10.1209/0295-5075/94/53001

16. F. Becker, Zerstörungsfreie Profilmessung intensiver Schwerionenstrahlen, Dissertation, TU-Darmstadt, (2010) https://tuprints.ulb.tu-darmstadt.de/2332/

17. W. Lichten, Molecular wave functions and inelastic atomic collisions. Phys. Rev. **164**, 131 (1967). https://doi.org/10.1103/PhysRev.164.131

18. T.J. Moratz, M.J. Kushner, Fission fragment pumping of a neon plasma. J. Appl. Phys. **63**, 1796 (1988). https://doi.org/10.1063/1.339872

19. R. Mann, S. Hagmann, L. Weitzel, Cusp-electrons used for velocity measurements of heavy ion projectiles. NIM B **34**, 403 (1988). https://doi.org/10.1016/0168-583X(88)90064-X

20. R. Laubert, S. Huldt, M. Breinig, L. Liljeby, S. Elston, R.S. Thoe, I.A. Sellin, Convoy electrons from solids in coincidence with emergent projectile charge state. J. Phys. B **14**, 859 (1981). https://doi.org/10.1088/0022-3700/14/5/019

21. A. Himpsl, T. Dandl, H. Hagn, A. Neumeier, W. Potzel, J. Wieser, A. Ulrich, Projectile-dependent scintillation of a liquid phase argon-xenon mixture. EPL **128**, 62002 (2019). https://doi.org/10.1209/0295-5075/128/62002

22. H. Deutsch, K. Becker, S. Matt, T.D. Märk, Theoretical determination of absolute electron-impact ionization cross sections of molecules. Int. J. Mass Spectrom. **197**, 37 (2000). https://doi.org/10.1016/S1387-3806(99)00257-2

23. D. Drouin, A. R. Couture, D. Joly, X. Tastet, V. Aimez, R. Gauvin, CASINO V2.42: a fast and easy-to-use modeling tool for scanning electron microscopy and microanalysis users, Universite de Sherbrooke, Canada, CASINO v. 2.51 (2017), https://doi.org/10.1002/sca.20000

24. A. Ulrich, *"Lichtemission und Lasereffekt bei Anregung mit ionisierender Strahlung", Habilitationsschrift, Fakultät für Physik* (Technische Universität München, Dezember, 1998)

25. G. Ribitzki, A. Ulrich, B. Busch, W. Krötz, J. Wieser, D.E. Murnick, Electron densities and temperatures in a xenon afterglow with heavy-ion excitation. Phys. Rev. E **50**, 3973 (1994). https://doi.org/10.1103/PhysRevE.50.3973

26. A. Ulrich, R. Gernhäuser, W. Krötz, J. Wieser, D.E. Murnick, Ion-atom charge-transfer system for a heavy-ion-beam pumped laser. Phys. Rev. A **50**, 1931 (1994). https://doi.org/10.1103/PhysRevA.50.1931

27. C.K. Rhodes (ed.), *Excimer Lasers, Topics in Applied Physics*, vol. 30 (Springer, Berlin, 1979)

28. R. Hampf, A. Ulrich, J. Wieser, Evaluation of CCD cameras for beam profile monitoring with high intensity particle beams traversing gases. EPJ Technol. Instrum. **7**, 5 (2020). https://doi.org/10.1140/epjti/s40485-020-00057-0

29. W. Krötz, A. Ulrich, B. Busch, G. Ribitzki, J. Wieser, Third excimer continuum of argon excited by a heavy-ion beam. Phys. Rev. A **43**, 6089 (1991). https://doi.org/10.1103/PhysRevA.43.6089

30. J. Wieser, A. Ulrich, A. Fedenev, M. Salvermoser, Novel pathways to the assignment of the third rare gas excimer continua. Opt. Commun. **173**, 233 (2000). https://doi.org/10.1016/S0030-4018(99)00610-0

31. A. Morozov, R. Krücken, T. Ottenthal, A. Ulrich, J. Wieser, Ultraviolet emission from argon water-vapor mixtures excited with low-energy electron beams. Appl. Phys. Lett. **86**, 011502 (2005)

32. Plasma Physics at FAIR: https://www.gsi.de/work/forschung/appamml/plasmaphysikphelix/hed_at_fair.htm

33. T. Dandl, T. Heindl, A. Ulrich, Fluorescence of nitrogen and air. J. Instrum. **7**, P11005 (2012). https://doi.org/10.1088/1748-0221/7/11/P11005

34. F. Becker, GSI annual report, 141 (2009)

35. A. Morozov, R. Krücken, J. Wieser, A. Ulrich, Gas kinetic studies using a table-top set-up with electron beam excitation: quenching of molecular nitrogen emission by water vapour. Eur. Phys. J. D **33**, 207 (2005). https://doi.org/10.1140/epjd/e2005-00051-7

36. A. Morozov, R. Krücken, A. Ulrich, J. Wieser, Energy-transfer processes in neon-hydrogen mixtures excited by electron beams. J. Chem. Phys. **123**, 234311 (2005). https://doi.org/10.1063/1.2134697

37. V.A. Ivanov, Dissociative recombination of molecular ions in noble-gas plasmas. Sov. Phys. Usp. **35**, 17 (1992). https://doi.org/10.1070/PU1992v035n01ABEH002192

38. M. Khasenov, Emission and level population in noble gases and their binary mixtures under ion beam excitation. NIM B **482**, 45 (2020). https://doi.org/10.1016/j.nimb.2020.09.004

39. A. Kramida et al., *NIST Atomic Spectra Database* (ver. 5.8), https://physics.nist.gov/asd [2021, January 19]. National Institute of Standards and Technology, Gaithersburg, MD. DOI: https://doi.org/10.18434/T4W30F

40. E. Schramm, A. Kürten, J. Hölzer, S. Mitschke, F. Mühlberger, M. Sklorz, J. Wieser, A. Ulrich, M. Pütz, R. Schulte-Ladbeck, R. Schultze, J. Curtius, S. Borrmann, R. Zimmermann, Trace detection of organic compounds in complex sample matrixes by single photon ionization ion trap mass spectrometry: real-time detection of security-relevant compounds and online analysis of the coffee-roasting process. Anal. Chem. **81**, 4456 (2009). https://doi.org/10.1021/ac900289r

41. A. Morozov, R. Krücken, A. Ulrich, Spatial distribution of fluorescent light emitted from neon and nitrogen excited by low energy electron beams. J. Appl. Phys. **100**, 093305 (2006). https://doi.org/10.1063/1.2374296

42. K. Shima et al., At. Data Nucl. Data Tables **51**, 173 (1992)